

We now examine the hydrogen atom cavities formed by the  $-C_2H_4-$  groups around the  $I_3^-$  anion in the  $\beta^*$ - and  $\alpha$ -phases. The stereodiagrams of Figure 5 depict how the ethylene group hydrogen atoms of one ET molecule in  $\beta^*-(ET)_2I_3$  and  $\alpha-(ET)_2I_3$  interact with the surrounding ET molecules and anions, respectively.<sup>21</sup> In  $\beta^*-(ET)_2I_3$ , three hydrogen atoms of each ethylene group have short contacts with the  $I_3^-$  anions (i.e., C-H...I interactions),<sup>7a</sup> while the remaining hydrogen atom sits on top of either a five- or six-membered ring of the adjacent ET molecule (i.e., C-H...S interactions). In  $\alpha-(ET)_2I_3$ , two hydrogen atoms of each ethylene group have short contacts with the  $I_3^-$  anions, and the other two hydrogen atoms have short contacts with sulfur and/or hydrogen atoms of the adjacent ET molecules. For every ethylene group, therefore,  $\beta^*-(ET)_2I_3$  always has more C-H... $I_3^-$  interactions than does  $\alpha-(ET)_2I_3$ . According to ab initio SCF-MO/MP2 calculations<sup>22</sup> on  $H_3C-H...I_3^-$  and  $H_3C-H...SH_2$  with the 6-311G\*\* quality basis set, the H...I and H...S contacts, respectively, have attractive interaction energies of 1.13 and 0.47 kcal/mol at their minimum-energy distances. Since  $\beta^*-(ET)_2I_3$  has more C-H... $I_3^-$  contacts than does  $\alpha-(ET)_2I_3$ , it may be speculated that  $\beta^*-(ET)_2I_3$  is thermodynamically more stable. This expectation is consistent with the conversion of  $\alpha-(ET)_2I_3$  to a  $\beta$ -like structure by thermal tempering.

- (21)  $\beta^*-(ET)_2I_3$  has one unique ET molecule,<sup>7</sup> but  $\alpha-(ET)_2I_3$  has three unique ET molecules (i.e., A, B, and C).<sup>9b</sup> Figure 5b shows the environment around molecule B. Molecules A and C have environments similar to that around molecule B.
- (22) Novoa, J. J.; Whangbo, M.-H.; Williams, J. M. To be submitted for publication.

## Concluding Remarks

The unusual  $\alpha$ - to  $\alpha_1-(ET)_2I_3$  (semiconductor to superconductor) thermal conversion has been monitored by use of a high-temperature ESR line width analysis technique. The ESR and FT-IR studies indicate that the  $\alpha_1$ -phase has a  $\beta$ -like structure. The superconducting  $T_c$  measurements, as well as Raman results,<sup>10d</sup> further suggest that the  $\alpha_1$ -phase is similar to structurally unique<sup>7,8</sup>  $\beta^*-(ET)_2I_3$ . The thermal conversion of  $\alpha$ - to  $\alpha_1-(ET)_2I_3$  implies that the  $\beta$ -like structure is thermodynamically more stable than the  $\alpha$ -structure. This appears to originate from the fact that the  $\beta$ -like structure allows more short contacts between donor-molecule hydrogen atoms and anions (i.e. C-H... $I_3^-$  contacts) than does the  $\alpha$ -structure. Thus, the thermal-tempering technique provides a convenient procedure for obtaining a large quantity of a  $\beta$ -like salt from a mixture of  $\alpha$ - and  $\beta$ -salts, which typically occurs during the electrocrystallization synthesis reaction.

**Acknowledgment.** Work at Argonne National Laboratory and North Carolina State University is supported by the U.S. Department of Energy, Office of Basic Energy Sciences, Division of Materials Sciences, under Contract W-31-109-ENG-38 and Grant DE-FG05-86ER45259, respectively. L.K.M. is a Scientist in Residence, sponsored by the Argonne Division of Educational Programs, on leave from the Department of Chemistry, Indiana University, Bloomington, IN. J.R.W. and J.A.S. are student research participants sponsored by the Argonne Division of Educational Programs from Transylvania University, Lexington, KY, and Valparaiso University, Valparaiso, IN, respectively.

Contribution from the Department of Chemistry, The University of North Carolina, Chapel Hill, North Carolina 27599-3290

## Effects of Conformational Change in the Acceptor on Intramolecular Electron Transfer

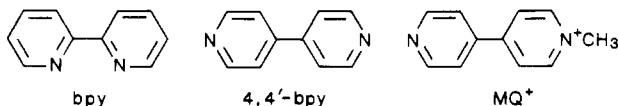
Pingyun Chen, Maria Curry, and Thomas J. Meyer\*

Received June 13, 1988

The structure of  $[(bpy)Re(CO)_3(MQ^+)](PF_6)_2$  (bpy is 2,2'-bipyridine;  $MQ^+$  is *N*-methyl-4,4'-bipyridinium cation) determined by X-ray diffraction shows that the complex is the *facial* isomer and is of distorted-octahedral geometry. The dihedral angle between the two pyridyl rings of the  $MQ^+$  ligand is  $47^\circ$  in the crystal. The similarities in  $d\pi \rightarrow \pi^*(MQ^+)$  transition energies in solution, in an organic glass, and in KBr pellets suggest that the dihedral angle between the two rings of the  $MQ^+$  ligand may be nearly medium-independent. The results of spectral and electrochemical studies on a series of complexes show the following: (1) the dihedral angle has a significant effect on the energies and intensities of the  $MQ^+$ -based metal to ligand charge-transfer (MLCT) transitions, (2) the relative ordering of the bpy- and  $MQ^+$ -based MLCT excited states in  $[(bpy)Re(CO)_3(MQ^+)]^{2+}$  depends upon the dihedral angle, and (3) changes in the dihedral angle and in solvent dipole reorientation play important roles in light-induced  $\pi^*(bpy) \rightarrow \pi^*(MQ^+)$  intramolecular electron transfer,  $[(bpy^*)Re^{II}(CO)_3(MQ^+)]^{2+*} \rightarrow [(bpy)Re^{II}(CO)_3(MQ^+)]^{2+*}$ .

### Introduction

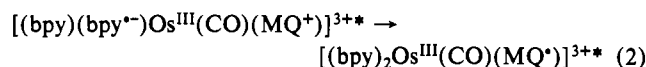
In chromophore-quencher (CQ) complexes where there is a metal to ligand charge-transfer (MLCT) excited state and a pyridinium electron-transfer acceptor, e.g.,  $[(bpy)_2Os(CO)-(MQ^+)]^{3+}$  (bpy is 2,2'-bipyridine,  $MQ^+$  is the *N*-methyl-4,4'-bipyridinium dication), a bpy-based MLCT emission is observed



at low temperatures in glasses, e.g., eq 1. The emissions are  $[(bpy)(bpy^*)Os^{III}(CO)(MQ^+)]^{3+*} \rightarrow [(bpy)_2Os^{II}(CO)(MQ^+)]^{3+} + h\nu$  (1)

comparable in energy and lifetime to the MLCT-based emission from related complexes such as  $[(bpy)_2Os(CO)(4,4'-bpy)]^{2+}$ .<sup>1,2</sup> However, in fluid solution, rapid intramolecular electron transfer occurs in the CQ complex to give a lower energy  $MQ^+$ -based excited state. The lower excited state is short-lived and emits weakly at room temperature.<sup>2</sup>

- (1) (a) Sullivan, B. P.; Abruna, H.; Finklea, H. O.; Salmon, D. J.; Nagle, J. K.; Meyer, T. J.; Sprintschnick, H. *Chem. Phys. Lett.* **1978**, *58*, 389. (b) Westmoreland, T. D.; Le Bozec, H. D.; Murray, R. W.; Meyer, T. J. *J. Am. Chem. Soc.* **1983**, *105*, 5952. (c) Nagle, J. K. Ph.D. Dissertation, The University of North Carolina, Chapel Hill, NC, 1979.
- (2) (a) Chen, P.-Y.; Danielson, E.; Meyer, T. J. *J. Phys. Chem.* **1988**, *92*, 3708. (b) Westmoreland, T. D.; Le Bozec, H. D.; Chen, P.-Y.; Danielson, E.; Meyer, T. J. Manuscript in preparation.



In bimolecular electron transfer, translational diffusion to form an association complex must occur prior to the electron-transfer event.<sup>3</sup> Since there is no requirement for translational diffusion in intramolecular electron transfer, a question arises as to why the intramolecular quenching event in reaction 2 is apparently "triggered" by solvent dynamics.

Related observations have been made in other chromophore-quencher complexes<sup>4</sup> and in the "TICT" states of organic donor-acceptor systems. In the organic systems light-induced electron transfer has been observed to induce conformational changes based on the relative orientations of the electron-transfer donor and acceptor.<sup>5</sup>

We have recently shown that in the glassy state both the free energy change and the loss of solvent dipole reorientations play important roles in determining whether or not intramolecular electron transfer can occur.<sup>2a</sup> Conformational changes are also expected to play a role in processes such as that shown in reaction 2. In biphenyl, which is structurally analogous to the MQ<sup>+</sup> ligand, the two phenyl rings adopt a nonpolar conformation in order to minimize the steric repulsion between the adjacent 2,2' and 6,6' hydrogen atoms on the two phenyl rings.<sup>6,7</sup> On the other hand,  $\pi$ - $\pi$  interactions between the rings, which are critically dependent upon the dihedral angle,<sup>8</sup> favor a planar conformation. In the ground state of biphenyl, there is a compromise between the two effects and the twisting angle is somewhat medium-dependent.<sup>7</sup> In both the lowest biphenyl  $\pi$ - $\pi^*$  excited state and in the 1-electron-reduced radical anion, the  $\pi$ - $\pi$  interactions between the rings are sufficiently strong that the inter-ring C-C bond assumes some double-bond character and the planar conformation is adopted.<sup>8,9</sup> Because of the conformational change that exists between the ground and excited states of biphenyl, its photo-physical properties are highly dependent upon solvent viscosity.<sup>9</sup>

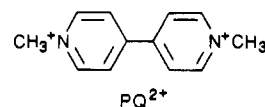
4,4'-Bipyridine assumes a nonplanar conformation or acts as a free rotor in solution.<sup>6c,10</sup> In its metal complexes, 4,4'-bpy can be either planar<sup>11</sup> or nonplanar.<sup>12</sup> PQ<sup>2+</sup> is also planar in the solid

**Table I.** Crystallographic Data for  $[(\text{bpy})\text{Re}(\text{CO})_3(\text{MQ}^+)](\text{PF}_6)_2$

formula	$[\text{Re}(\text{C}_{24}\text{O}_3\text{N}_4\text{H}_{19})](\text{PF}_6)_2$
space group	$P2_1/a$
fw	887.57
$a$ , Å	14.910 (3)
$b$ , Å	11.270 (2)
$c$ , Å	19.264 (1)
$\beta$ , deg	109.85 (1)
$V$ , Å <sup>3</sup>	3044.7
$Z$	4
$D_c$ , g cm <sup>-3</sup>	1.936
$D_o$ , g cm <sup>-3</sup>	1.900
data range, deg	$2 \leq \theta(M_0) \leq 24$
$R$	0.054
$R_w$	0.047
NO [ $I > 3\sigma(I)$ ] <sup>a</sup>	2038
NO	5206
quality of fit indicator	1.669
largest shift/esd, final cycle	0.63

<sup>a</sup>NO = number of observations.

state.<sup>13</sup> In the 1-electron-reduced form of the *N,N'*-dimethyl-4,4'-bipyridinium cation, PQ<sup>2+</sup>,<sup>14</sup> and in the 4,4'-bpy radical an-



ion,<sup>15</sup> electronic coupling between the rings is sufficient to overcome the H-H repulsion and both ions are planar. This also appears to be the case for MQ<sup>+</sup>-based MLCT excited states such as  $[(\text{bpy})_2\text{Os}^{\text{III}}(\text{CO})(\text{MQ}^+)]^{3+*}$  or  $[(\text{bpy})\text{Re}^{\text{II}}(\text{CO})_3(\text{MQ}^+)]^{2+*}$ .<sup>2</sup> Transient absorption spectra of these excited states show the appearance of a low-energy absorption feature at  $\sim 600$  nm that appears to be a characteristic feature of the ring-delocalized structure.

In the MQ<sup>+</sup>-based CQ complexes, the rate of the intramolecular  $\pi^*(\text{bpy}) \rightarrow \pi^*(\text{MQ}^+)$  electron transfer or even the appearance of quenching is expected to be influenced by the dihedral angle of the MQ<sup>+</sup> acceptor. The ability of the ligand as an electron acceptor should be dependent upon the dihedral angle. Reduction of *N*-methylpyridinium ion ( $E_{1/2} = -1.21$  V in acetonitrile vs SSCE)<sup>16</sup> is more difficult than reduction of MQ<sup>+</sup> ( $E_{1/2} = -0.96$  V)<sup>17</sup> mainly because of  $\pi^*-\pi^*$  electronic delocalization onto the second ring for MQ<sup>+</sup>. A dynamic effect could also exist. If the two rings are highly twisted and electronic coupling is weak in the ground state, rotation to the planar conformation must occur upon reduction. If the rotation is the slowest vibrational change required in the electron-transfer event, its dynamics would dictate the temporal characteristics of the preexponential term for electron transfer.

Solvent dipole reorientations also play an important role in the intramolecular electron transfer process. In the intramolecular electron transfer in reaction 2 there is a considerable change in radial electronic distribution. The solvent dipole reorientations that occur in association with the electron transfer are rapid in fluid solution. In a glass they are frozen. The solvent dipoles are

- (3) (a) Meyer, T. J. *Prog. Inorg. Chem.* **1983**, *30*, 389. (b) Newton, M. D.; Sutin, N. *Annu. Rev. Phys. Chem.* **1984**, *35*, 437. (c) Mataga, N. *J. Mol. Struct. (THEOCHEM)* **1986**, *135*, 279.
- (4) (a) Westmoreland, T. D.; Schanze, K. S.; Neveux, Jr., P. E.; Danielson, E.; Sullivan, B. P.; Chen, P.-Y.; Meyer, T. J. *Inorg. Chem.* **1985**, *24*, 2596. (b) Chen, P.-Y.; Westmoreland, T. D.; Danielson, E.; Schanze, K. S.; Anthon, D.; Neveux, P. E.; Meyer, T. J. *Inorg. Chem.* **1987**, *26*, 1116.
- (5) (a) Rettig, W. J. *Lumin.* **1980**, *26*, 21. (b) Kallir, A. J.; Suter, G. W.; Wild, U. P. *J. Phys. Chem.* **1987**, *91*, 60. (c) Grabowsky, Z. R.; Rotkiewicz, K.; Siemiarczuk, A. *J. Lumin.* **1979**, *18/19*, 420. (d) Dobkowski, J.; Kirkor-Kaminska, E.; Koput, J.; Siemiarczuk, A. *J. Lumin.* **1982**, *27*, 339. (e) Itoh, K.; Azumi, T. *J. Chem. Phys.* **1975**, *62*, 3431. (f) Krygowski, T. M. *J. Chem. Res., Synop.* **1987**, 120.
- (6) (a) Almenning, A.; Bastiansen, O.; Fernholt, L.; Cyvin, B.; Cyvin, S. J.; Samdal, S. *J. Mol. Struct. (THEOCHEM)* **1985**, *128*, 59. (b) Bastiansen, O.; Samdal, S. *J. Mol. Struct. (THEOCHEM)* **1985**, *128*, 115. (c) Maier, J. P.; Turner, D. W. *Faraday Discuss. Chem. Soc.* **1972**, *54*, 149.
- (7) (a) Schaefer, T.; Peeling, J.; Penner, G. H. *Can. J. Chem.* **1986**, *64*, 2162. (b) Eaton, V. J.; Steele, D. *J. Chem. Soc., Faraday Trans. 2* **1973**, 1601. (c) Suzuki, H. *Bull. Chem. Soc. Jpn.* **1959**, *32*, 1340.
- (8) (a) Imamura, A.; Hoffmann, R. *J. Am. Chem. Soc.* **1968**, *90*, 5379. (b) Momicchioli, F.; Bruni, M. C.; Baraldi, I. *J. Phys. Chem.* **1972**, *76*, 3983. (c) Takahashi, C.; Maeda, S. *Chem. Phys. Lett.* **1974**, *24*, 584. (d) Yamaguchi, S.; Yamimizu, N.; Maeda, S. *J. Phys. Chem.* **1978**, *82*, 1078.
- (9) (a) Cooke, B. J.; Palmer, T. F. *J. Photochem.* **1984**, *26*, 149. (b) Naqvi, K. R.; Donatsch, J.; Wiler, U. P. *Chem. Phys. Lett.* **1975**, *34*, 285. (c) Fujii, T.; Suzuki, S.; Komatsu, S. *Chem. Phys. Lett.* **1978**, *57*, 175.
- (10) (a) Galasso, V.; Alti, G. D.; Bigotto, A. *Tetrahedron* **1971**, *27*, 991. (b) Emsley, J. W.; Stephenson, D. S.; Lindon, J. C.; Lunizzi, L.; Pulga, S. *J. Chem. Soc., Perkin Trans. 2* **1975**, 1541. (c) Spotswood, T. M.; Tanzer, C. I. *Aust. J. Chem.* **1967**, *20*, 1227.
- (11) (a) Kubel, F.; Strohle, J. *Z. Naturforsch., B: Anorg. Chem., Org. Chem.* **1982**, *B37*, 272. (b) Julve, M.; Verdager, M.; Faus, J.; Tinti, F.; Moratal, J.; Monge, A.; Gutierrez-Puebla, E. *Inorg. Chem.* **1987**, *26*, 3520.
- (12) (a) Stephens, F. S.; Vagg, R. S. *Inorg. Chim. Acta* **1982**, *42*, 139. (b) Bukowska-Strzyzewska, M.; Tosik, A. *Acta Crystallogr., Sect. B* **1982**, *B38*, 265, 950.
- (13) (a) Bukowska-Strzyzewska, M.; Tosik, A. *Pol. J. Chem.* **1979**, *53*, 2423. (b) Russel, J. H.; Wallwork, S. C. *Acta Crystallogr., Sect. B* **1972**, *28*, 1527; **1969**, *B25*, 1691. (c) Mahmoud, M. M.; Wallwork, S. C. *Acta Crystallogr., Sect. B* **1976**, *B32*, 440. (d) Allwood, B. L.; Spencer, N.; Shariari-Zavareh, H.; Stoddart, J. F.; Williams, D. J. *J. Chem. Soc., Chem. Commun.* **1987**, 1064.
- (14) (a) Hester, R. E.; Suzuki, S. *J. Phys. Chem.* **1982**, *86*, 4626. (b) Johnson, C. S.; Gutowsky, H. S. *J. Chem. Phys.* **1963**, *39*, 58. (c) Hoffmann, H. J.; Cimiriaglia, R.; Tomasi, J. *J. Chem. Res., Synop.* **1987**, 48.
- (15) (a) Kihara, H.; Gondo, Y. *J. Raman Spectrosc.* **1986**, *17*, 263. (b) Barker, D. J.; Cooney, R. P.; Summers, L. A. *J. Raman Spectrosc.* **1987**, *18*, 443. (c) Hennig, J. C. M. *J. Chem. Phys.* **1966**, *44*, 2139.
- (16) Mackay, R. A.; Landolph, J. R.; Poziomek, E. *J. Am. Chem. Soc.* **1971**, *93*, 5026.
- (17) Curtis, J. C.; Sullivan, B. P.; Meyer, T. J. *Inorg. Chem.* **1983**, *22*, 224.

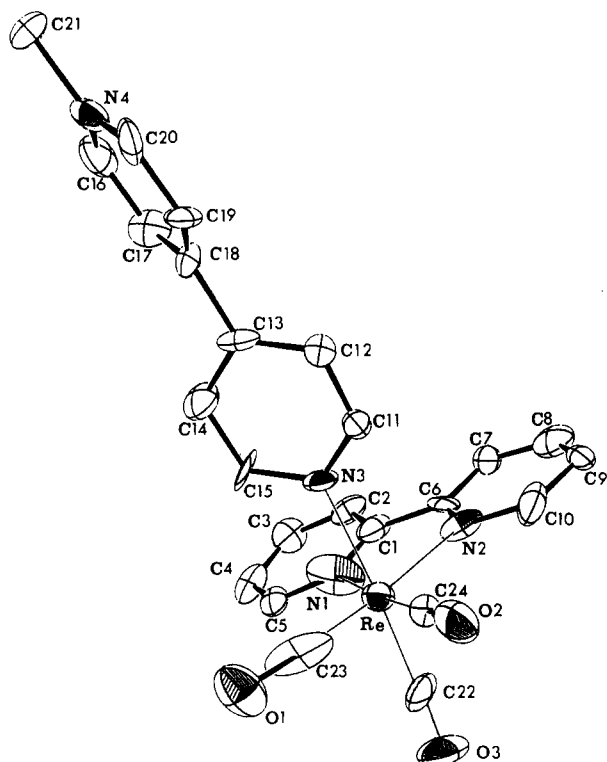
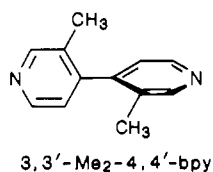


**Figure 1.** ORTEP diagram for  $[(bpy)Re(CO)_3(MQ^+)](PF_6)_2$ . The structure is oriented so as to show the relative orientation of the two pyridine rings of the  $MQ^+$  ligand.

locked into orientations that are appropriate to the electronic distribution of the ground state. Unless the free energy released is larger than the barrier imposed by the solvent dipole reorientations, intramolecular electron transfer can not occur.<sup>2a</sup>

In this paper, we have attempted to resolve the question of the role of ring-ring dihedral angle changes in bipyridinium-based CQ complexes. Our conclusions are based on crystallographic data for the complex  $[(bpy)Re(CO)_3(MQ^+)](PF_6)_2$ , and on spectral and electrochemical comparisons. The comparisons involve complexes of Os(II), Re(I), and Ru(II) that contain the ligands 4,4'-bipyridine, 3,3'-dimethyl-4,4'-bipyridine (3,3'-Me<sub>2</sub>-4,4'-bpy), or their methylated or protonated forms.



### Experimental Section

The preparations, characterizations, and detailed spectral and electrochemical properties of the complexes are to be published elsewhere.<sup>2b</sup> The crystal used in the X-ray diffraction study was grown by slowly cooling to room temperature a methanol solution containing  $[(bpy)Re(CO)_3(MQ^+)](PF_6)_2$ , which had been heated to reflux. This process gave small crystals. Larger crystals were obtained a few days later by slow evaporation of additional methanol at room temperature. The crystals were collected, rinsed with a small amount of methanol, and dried in a vacuum desiccator.

Acetonitrile used for spectral and electrochemical measurements was Burdick and Jackson spectroquality. Ethanol for temperature-dependent studies was freshly distilled over Mg/I<sub>2</sub>. Methanol (Burdick and Jackson) was used as received.

UV-visible absorption spectra were recorded on a HP8451A diode-array spectrophotometer. Low-temperature spectra were taken in an Oxford Cryostat with an Oxford 3120 automatic temperature controller. Solid-state absorption spectra were obtained on KBr pellets and corrected for light scattering by subtracting the spectrum of a blank pellet prepared in a similar manner. In order to account for variations in thickness and smoothness of the pellets, the blank spectrum was multiplied by a scaling factor so that the absorbance of the corrected spectrum was zero in

**Table II.** Atomic Positional Parameters for  $[(bpy)Re(CO)_3(MQ^+)](PF_6)_2$  According to the Numbering Scheme in Figure 1

atom	x	y	z
Re	-0.22628 (5)	-0.22409 (7)	0.21925 (5)
P(1)	-0.7453 (3)	-0.2591 (5)	-0.1267 (3)
P(2)	-0.3085 (4)	0.0813 (5)	0.4424 (3)
F(1)	-0.8427 (7)	-0.193 (1)	-0.1375 (6)
F(2)	-0.7479 (8)	-0.313 (1)	-0.0520 (6)
F(3)	-0.6856 (8)	-0.152 (1)	-0.0808 (6)
F(4)	-0.6489 (7)	-0.326 (1)	-0.1165 (6)
F(5)	-0.7447 (8)	-0.204 (1)	-0.2038 (6)
F(6)	-0.8039 (7)	-0.368 (1)	-0.1736 (6)
F(7)	-0.3445 (11)	0.158 (1)	0.3739 (7)
F(8)	-0.2966 (10)	0.197 (1)	0.4870 (8)
F(9)	-0.4094 (9)	0.070 (1)	0.4456 (11)
F(10)	-0.3203 (11)	-0.031 (1)	0.3968 (8)
F(11)	-0.2707 (8)	0.005 (1)	0.5145 (7)
F(12)	-0.2041 (8)	0.093 (1)	0.4473 (9)
O(1)	-0.1210 (8)	-0.118 (1)	0.3717 (7)
O(2)	-0.0643 (9)	-0.402 (1)	0.2726 (8)
O(3)	-0.0980 (9)	-0.080 (1)	0.1556 (8)
N(1)	-0.3078 (8)	-0.290 (1)	0.1142 (7)
N(2)	-0.3513 (9)	-0.113 (1)	0.1795 (7)
N(3)	-0.3169 (8)	-0.341 (1)	0.2629 (7)
N(4)	-0.5590 (8)	-0.744 (1)	0.4097 (6)
C(22)	-0.149 (1)	-0.131 (2)	0.1795 (11)
C(23)	-0.165 (1)	-0.157 (2)	0.3082 (9)
C(24)	-0.128 (1)	-0.327 (2)	0.2513 (11)
C(1)	-0.395 (1)	-0.242 (2)	0.0791 (8)
C(2)	-0.456 (1)	-0.288 (2)	0.0111 (9)
C(3)	-0.431 (1)	-0.380 (2)	-0.0216 (10)
C(4)	-0.341 (1)	-0.428 (2)	0.0122 (9)
C(5)	-0.287 (1)	-0.381 (2)	0.0763 (9)
C(6)	-0.414 (1)	-0.140 (2)	0.1181 (9)
C(7)	-0.502 (1)	-0.075 (2)	0.0849 (10)
C(8)	-0.514 (1)	0.022 (2)	0.1217 (11)
C(9)	-0.450 (1)	0.053 (2)	0.1898 (11)
C(10)	-0.364 (1)	-0.017 (2)	0.2184 (10)
C(11)	-0.333 (1)	-0.455 (2)	0.2389 (10)
C(12)	-0.380 (1)	-0.535 (2)	0.2690 (10)
C(13)	-0.418 (1)	-0.495 (2)	0.3200 (9)
C(14)	-0.401 (1)	-0.376 (1)	0.3441 (10)
C(15)	-0.351 (1)	-0.306 (1)	0.3141 (9)
C(16)	-0.495 (1)	-0.672 (1)	0.4559 (10)
C(17)	-0.449 (1)	-0.589 (2)	0.4295 (9)
C(18)	-0.466 (1)	-0.581 (1)	0.3561 (10)
C(19)	-0.533 (1)	-0.653 (2)	0.3092 (9)
C(20)	-0.579 (1)	-0.738 (2)	0.3370 (10)
C(21)	-0.609 (1)	-0.836 (2)	0.4407 (12)

regions where the solution spectrum has no absorbance.

**X-ray Data Collection.** X-ray crystallographic data were obtained by using a translucent light yellow, rectangularly shaped prism of approximate dimensions of 0.5 × 0.3 × 0.3 mm. All data were collected on an Enraf-Nonius Cad 4 diffractometer by using Mo K $\alpha$  radiation from 2 $^\circ$  < 2 $\theta$  < 44 $^\circ$  and a Zr filter. Methods for data collection and reduction have been described previously.<sup>18</sup> Lattice parameters obtained from a least-squares analysis of the angular settings for 25 reflections were  $a = 14.910$  (3) Å,  $b = 11.270$  (3) Å,  $c = 19.264$  (2) Å, and  $\beta = 109.85$  (1) $^\circ$  and are summarized along with other crystallographic data in Table I.

**Solution and Refinement of the Structure.** The position of the Re atom was determined from the Patterson function, and the positions of all other non-hydrogen atoms were obtained from difference Fourier maps. Positions for the hydrogen atoms were calculated from the planar geometries of the carbon atoms in  $MQ^+$  and the bipyridine rings by assuming a C-H bond distance of 0.95 Å. The atomic scattering factors were obtained from ref 19. The intensity data were corrected for Lorentz polarization effects but not for absorption. A weighting scheme described by Ibers and co-workers<sup>20</sup> was used with a weighting factor of  $P = 0.02$ . In the final least-squares calculation there were 415 variables and 2038 observations; the largest parameter shift was 0.63.

(18) Graves, B. J.; Hodgson, D. J. *Acta Crystallogr., Sect. B* **1982**, *B32*, 135.

(19) Hamilton, W. C.; Ibers, J. A. Eds. *International Tables for X-Ray Crystallography*; Kynoch Press: Birmingham, England, 1984; Vol. IV.

(20) Corfield, P. W. R.; Dordens, R. J.; Ibers, J. A. *Inorg. Chem.* **1967**, *6*, 197.

**Table III.** Bond Lengths (Å) in  $[(\text{bpy})\text{Re}(\text{CO})_3(\text{MQ}^+)](\text{PF}_6)_2$  According to the Numbering Scheme in Figure 1

Re-N(1)	2.11 (1)	C(1)-N(1)	1.36 (1)
Re-N(2)	2.16 (1)	C(1)-C(2)	1.41 (2)
Re-N(3)	2.24 (1)	C(1)-C(6)	1.46 (2)
Re-C(22)	1.90 (1)	C(2)-C(3)	1.34 (2)
Re-C(23)	1.81 (2)	C(3)-C(4)	1.38 (2)
Re-C(24)	1.80 (2)	C(4)-C(5)	1.34 (2)
		C(5)-N(1)	1.35 (1)
P(1)-F(1)	1.580 (9)	C(6)-N(2)	1.27 (1)
P(1)-F(2)	1.575 (9)	C(6)-C(7)	1.44 (2)
P(1)-F(3)	1.58 (1)	C(7)-C(8)	1.34 (2)
P(1)-F(4)	1.58 (1)	C(8)-C(9)	1.38 (2)
P(1)-F(5)	1.61 (1)	C(9)-C(10)	1.44 (2)
P(1)-F(6)	1.597 (9)	C(10)-N(2)	1.37 (2)
P(2)-F(7)	1.51 (1)	C(11)-N(3)	1.36 (1)
P(2)-F(8)	1.54 (1)	C(11)-C(12)	1.38 (2)
P(2)-F(9)	1.53 (1)	C(12)-C(13)	1.36 (2)
P(2)-F(10)	1.51 (1)	C(13)-C(14)	1.42 (1)
		C(13)-C(18)	1.51 (2)
P(2)-F(11)	1.57 (1)	C(14)-C(15)	1.34 (1)
P(2)-F(12)	1.53 (1)	C(15)-N(3)	1.31 (1)
		C(16)-N(4)	1.34 (1)
C(22)-O(3)	1.16 (1)	C(16)-C(17)	1.35 (1)
C(23)-O(1)	1.25 (2)	C(17)-C(18)	1.35 (2)
C(24)-O(2)	1.23 (2)	C(18)-C(19)	1.37 (2)
		C(19)-C(20)	1.38 (2)
		C(20)-N(4)	1.33 (1)

## Results

**X-ray Crystal Structure of  $[(\text{bpy})\text{Re}(\text{CO})_3(\text{MQ}^+)](\text{PF}_6)_2$ .** The geometry of  $[(\text{bpy})\text{Re}(\text{CO})_3(\text{MQ}^+)](\text{PF}_6)_2$  as it appears in the crystal is shown in the ORTEP diagram in Figure 1. The structure shows that the coordination geometry at Re is the facial isomer of an approximate octahedron.<sup>21</sup>

The positional parameters are listed in Table II, and the anisotropic thermal parameters are given in supplementary Table S1. A listing of hydrogen atom positions is also available as supplementary material. The important bond lengths and bond angles are collected in Tables III and IV.

Of interest in the context of the charge-transfer properties of the complex is the relative disposition of the two pyridine rings of the  $\text{MQ}^+$  ligand. In the structure in Figure 1, the dihedral angle between the two pyridyl rings is  $47^\circ$ . The C(13)-C(18) inter-ring bond distance is 1.51 (2) Å.

At the metal center the trans angles formed by Re(I) and two coordinated atoms trans to each other range from  $174.6$  to  $177.3^\circ$ , showing a slight deviation from ideal octahedral geometry. The Re-C-O angles range from  $175$  to  $176^\circ$ . The bond angles for N(1)-Re-N(3) and N(2)-Re-N(3) are smaller than  $90^\circ$  as are the angles formed between Re and the carbon atoms of the three CO groups. The net effect is to give a distortion toward a twisted triangular prism with the three nitrogen atoms of the pyridine groups and three carbon atoms of the carbonyl groups forming the two triangular planes. A similar distortion has been found in related complexes.<sup>21</sup>

The bond lengths are within normal ranges found in related structures,<sup>21</sup> but there are some features that are worth noting. (1) The Re-N(1) and Re-N(2) bond lengths to bpy differ by 0.05 Å although there is no reason to believe that they are not chemically equivalent. This may be a crystal packing effect caused by the unsymmetrical packing of the  $\text{PF}_6^-$  counterion near the pyridine rings. (2) The Re-N(MQ<sup>+</sup>) bond is longer by 0.11 Å than is the average Re-N(bpy) bond distance. (3) The Re-C(22) bond, which is trans to MQ<sup>+</sup>, is longer than the other two Re-C bonds by 0.09 Å, and the C-O bond distance is shorter by 0.08 Å.

**Electrochemistry.** Reduction potentials for several free pyridinium ions and for the pyridinium quencher sites in the CQ

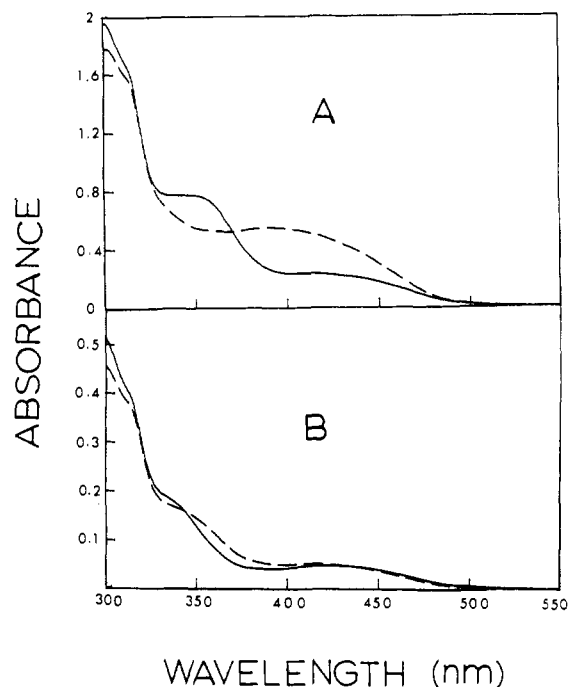


**Figure 2.** Absorption spectra in acetonitrile of (A)  $[(\text{bpy})_2\text{Os}(\text{CO})(4,4'\text{-bpy})]^{2+}$  (—) and  $[(\text{bpy})_2\text{Os}(\text{CO})(4,4'\text{-bpyH}^+)]^{3+}$  (---) and (B)  $[(\text{bpy})_2\text{Os}(\text{CO})(3,3'\text{-Me}_2\text{-}4,4'\text{-bpy})]^{2+}$  (—) and  $[(\text{bpy})_2\text{Os}(\text{CO})(3,3'\text{-Me}_2\text{-}4,4'\text{-bpyH}^+)]^{3+}$  (---). The spectra of the protonated complexes were obtained by adding 2–3 drops of aqueous  $\text{HPF}_6$  to the solutions.

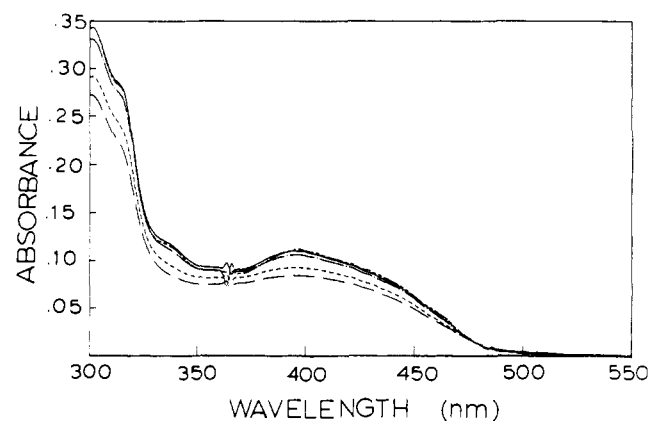


**Figure 3.** Absorption spectra of  $[(\text{bpy})_2\text{Os}(\text{CO})(\text{MQ}^+)]^{3+}$  in 4:1 EtOH/MeOH at (---) 295, (-.-) 200, (-·-) 150, (—) 130, and (- - -) 100 K.

complexes are collected in Table V.<sup>2b,16,17,22</sup> For comparison, reduction potentials for bpy-based model complexes are also included. The reduction potentials for the pyridinium ions of different structure differ considerably.

**UV-Visible Absorption Spectra.** The UV-visible absorption spectra of  $[(\text{bpy})_2\text{Os}(\text{CO})(4,4'\text{-bpy})]^{2+}$  and its protonated form,  $[(\text{bpy})_2\text{Os}(\text{CO})(4,4'\text{-bpyH}^+)]^{3+}$ , in acetonitrile solution at room temperature are shown in Figure 2A. Spectra of the methylated analogue  $[(\text{bpy})_2\text{Os}(\text{CO})(\text{MQ}^+)]^{3+}$  in 4:1 (v/v) EtOH/MeOH at a series of temperatures are shown in Figure 3. The glitch at 365 nm is an instrumental artifact. The same spectral features appear in acetonitrile solution as in the alcohol mixture but are slightly shifted.  $\lambda$  values and spectral assignments for the MLCT transitions in a series of complexes are given in Table VI.

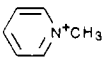
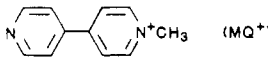
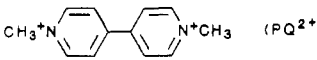
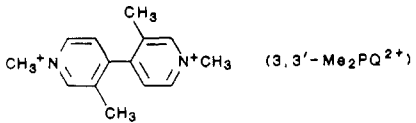
The spectra in Figure 2A show that significant changes occur when an electron acceptor site is introduced into the chromophore by means of protonation or methylation of the uncoordinated nitrogen atom on the remote pyridine ring of 4,4'-bpy. By contrast,

(21) (a) Horn, E.; Snow, M. R. *Aust. J. Chem.* **1980**, *33*, 2369. (b) Buchner, S.; Cotton, F. A.; Falvello, L. R.; Reid, A. H.; Schmulbach, C. D. *Inorg. Chem.* **1986**, *25*, 1021. (c) Calabrese, J. C.; Tam, W. *Chem. Phys. Lett.* **1987**, *133*, 244. (d) Cotton, F. A.; Daniels, L. M. *Acta Crystallogr., Sect. C* **1983**, *C39*, 1495.

(22) Megehee, E. B. G. Ph.D. Dissertation, The University of North Carolina, Chapel Hill, 1986.



**Table V.** Reduction Potentials for Bound and Free Pyridinium Ions in Acetonitrile,  $\mu = 0.1$  M, vs SSCE<sup>a</sup>

ions or complexes	$E_{1/2}(1)$ , V	$E_{1/2}(2)$ , V	$E_{1/2}(\text{bpy}^{0/-})$ , V
	-1.21 <sup>b</sup>		
 (MQ <sup>+</sup> )	-0.96 <sup>c</sup>		
 (PQ <sup>2+</sup> )	-0.46	-0.87 <sup>d</sup>	
 (3,3'-Me <sub>2</sub> PQ <sup>2+</sup> )	-0.78	-1.00	
[(bpy) <sub>2</sub> Os(CO)(py)] <sup>2+</sup>			-1.15 <sup>e</sup>
[(bpy) <sub>2</sub> Os(CO)(MQ <sup>+</sup> )] <sup>3+</sup>	-0.68		-1.12 <sup>f</sup>
[(bpy) <sub>2</sub> Os(CO)(3,3'-Me <sub>2</sub> MQ <sup>+</sup> )] <sup>3+</sup>	-1.04		-1.13 <sup>f</sup>
[(bpy)Re(CO) <sub>3</sub> (4-Etpy)] <sup>+</sup>			-1.17 <sup>g</sup>
[(MQ <sup>+</sup> ) <sub>2</sub> Re(CO) <sub>3</sub> Cl] <sup>2+</sup>	-0.76 <sup>f,g</sup>		
[(bpy)Re(CO) <sub>3</sub> (MQ <sup>+</sup> )] <sup>2+</sup>	-0.68 <sup>f</sup>	-1.17 <sup>f</sup>	

<sup>a</sup>  $E_{1/2}$  calculated from the average of cathodic and anodic peak potentials in cyclic voltammograms obtained in a one-compartment cell at a scan rate of 200 mV/s. The counterion was PF<sub>6</sub><sup>-</sup> and the supporting electrolyte was [N(n-C<sub>4</sub>H<sub>9</sub>)<sub>4</sub>](PF<sub>6</sub>). <sup>b</sup> Reference 16. <sup>c</sup> Reference 17. <sup>d</sup> Reference 30. <sup>e</sup> Reference 23. <sup>f</sup> Reference 2. <sup>g</sup> Two-electron reduction wave.

**Table VI.**  $\lambda_{\text{max}}$  Values and Spectral Assignment for MLCT Transitions in Acetonitrile at 22 ± 2 °C

complex	$\lambda_{\text{max}}$ , nm	
	$d\pi \rightarrow \pi^*(\text{bpy})$	$d\pi \rightarrow \pi^*(4,4'\text{-bpy or MQ}^+)$
[(bpy) <sub>2</sub> Os(CO)(py)] <sup>2+</sup>	420	
[(bpy) <sub>2</sub> Os(CO)(4,4'-bpy)] <sup>2+</sup>	412	355 <sup>a</sup>
[(bpy) <sub>2</sub> Os(CO)(MQ <sup>+</sup> )] <sup>3+</sup>	420 <sup>b</sup>	390 <sup>b</sup>
[(bpy) <sub>2</sub> Os(CO)(3,3'-Me <sub>2</sub> -4,4'-bpy)] <sup>2+</sup>	416	335 <sup>a</sup>
[(bpy) <sub>2</sub> Os(CO)(3,3'-Me <sub>2</sub> MQ <sup>+</sup> )] <sup>3+</sup>	414	350 <sup>a</sup>
[(bpy)Re(CO) <sub>3</sub> (4-Etpy)] <sup>+</sup>	350	
[(bpy)Re(CO) <sub>3</sub> (4,4'-bpy)] <sup>+</sup>	350	315 <sup>b</sup>
[(bpy)Re(CO) <sub>3</sub> (3,3'-Me <sub>2</sub> -4,4'-bpy)] <sup>+</sup>	350	
[(bpy)Re(CO) <sub>3</sub> (MQ <sup>+</sup> )] <sup>2+</sup>	350 <sup>b</sup>	340 <sup>b</sup>
[(MQ <sup>+</sup> )Re(CO) <sub>3</sub> Cl] <sup>2+</sup>		355

<sup>a</sup> Estimated, since the absorption feature appears as a shoulder.

<sup>b</sup> The bands are strongly overlapped and were resolved by a spectral resolution procedure; see the text for details.

to separate the overlapped transitions. The spectra were obtained as the differences between the spectra of 4,4'-bpy-based complexes and [(bpy)Re(CO)<sub>3</sub>(4-Etpy)]<sup>+</sup> as a means of subtracting out the  $d\pi \rightarrow \pi^*(\text{bpy})$  and  $\pi \rightarrow \pi^*(\text{bpy})$  components. The difference spectra are shown in the inset in the upper right corner in Figure 4. The spectra show that the  $d\pi \rightarrow \pi^*(4,4'\text{-bpy})$  transition at 306 nm is shifted to 336 nm for the  $d\pi \rightarrow \pi^*(\text{MQ}^+)$  transition. This shift, ~2900 cm<sup>-1</sup>, is comparable to the shift observed for the analogous Os(II) complexes,  $\Delta\nu_{\text{max}} \sim 2500$  cm<sup>-1</sup> (vide infra).

The spectra of [(MQ<sup>+</sup>)<sub>2</sub>Re(CO)<sub>3</sub>Cl]<sup>2+</sup> and of [(bpy)Re(CO)<sub>3</sub>(MQ<sup>+</sup>)]<sup>2+</sup> in a 4:1 EtOH/MeOH solution at different temperatures are shown in Figure 5. The spectrum of the (MQ<sup>+</sup>)<sub>2</sub> complex is free of bpy-based  $\pi \rightarrow \pi^*$  and MLCT transitions, and a well-resolved  $d\pi \rightarrow \pi^*(\text{MQ}^+)$  transition appears at 355 nm.<sup>23</sup>

The spectra of [(bpy)Re(CO)<sub>3</sub>(MQ<sup>+</sup>)](PF<sub>6</sub>)<sub>2</sub> and [(bpy)Re(CO)<sub>3</sub>(4,4'-bpy)](PF<sub>6</sub>)<sub>2</sub> and the difference spectrum between them, all in KBr pellets, are shown in Figure 6. The glitch at 320 nm in the difference spectrum arises from slight shifts in the  $\pi \rightarrow \pi^*(\text{bpy})$  transitions between the two complexes. The same spectral features appear in KBr pellets as in solution for these complexes and for [(bpy)<sub>2</sub>Os(CO)(MQ<sup>+</sup>)](PF<sub>6</sub>)<sub>3</sub> and [(MQ<sup>+</sup>)<sub>2</sub>Re(CO)<sub>3</sub>Cl](PF<sub>6</sub>)<sub>2</sub> except that absorption bandwidths are slightly broader.

## Discussion

The focus of this paper is on how the relative orientations of the pyridyl rings in the MQ<sup>+</sup> ligand influence it as an electron

acceptor. Some useful conclusions can be drawn based on the crystal structure of [(bpy)Re(CO)<sub>3</sub>(MQ<sup>+</sup>)](PF<sub>6</sub>)<sub>2</sub>, comparisons among spectra obtained in solution, the glassy state, or the solid state, and electrochemical data. It is convenient first to consider the insight into electronic structure that can be found in the molecular structure of the cation [(bpy)Re(CO)<sub>3</sub>(MQ<sup>+</sup>)]<sup>2+</sup>.

**Structure of [(bpy)Re(CO)<sub>3</sub>(MQ<sup>+</sup>)](PF<sub>6</sub>)<sub>2</sub>.** The bond lengths of both the Re-N(MQ<sup>+</sup>) bond and the Re-C bond of the carbonyl ligand trans to MQ<sup>+</sup> are relatively long. The structure is sufficiently open that steric effects can hardly play a role. The lengthening is an electronic effect arising from competitive  $d\pi-\pi^*(\text{CO})$  and  $d\pi-\pi^*(\text{MQ}^+)$  back-bonding. There is a low-lying  $\pi^*$  acceptor level in MQ<sup>+</sup>. In the ion [(NH<sub>3</sub>)<sub>3</sub>Ru<sup>II</sup>(Mepz<sup>+</sup>)]<sup>3+</sup> (Mepz<sup>+</sup> is *N*-methylpyrazinium cation), where there is no trans competition for back-bonding, the Ru-N(Mepz<sup>+</sup>) bond distance is short.<sup>24</sup>

Crystallographic data are available concerning the dihedral angle between the two pyridyl rings in diquaternized 4,4'-bipyridinium dications<sup>13</sup> and in metal complexes in which 4,4'-bpy is a bridging ligand.<sup>11,12</sup> The *N,N'*-dialkyl-4,4'-bipyridinium cations tend to adopt a planar conformation in crystals, but there is no preferred conformation for 4,4'-bpy as a bridging ligand. The dihedral angle defining the relative orientations of the two pyridine rings ranges from 0 to 40°.<sup>11,12</sup>

In the solid state the three factors that influence the dihedral angles are crystal packing, steric repulsion by the H atoms in the 3,3'- and 5,5'-positions of the rings, and electronic coupling between the  $\pi$  systems of the two rings. Only the latter two factors are important in solution. Steric repulsion is minimized at a dihedral angle of 90° and maximized at 0° while the opposite is true for electronic coupling between the rings.<sup>6,9,11-13</sup> For 4,4'-bpy as bridging ligand, an additional electronic factor is  $d\pi-\pi^*(\text{MQ}^+)$  mixing,<sup>11,12</sup> which is maximized as the dihedral angle approaches 0°.

The resonance stabilization energy arising from  $\pi$  interactions between the rings depends upon the extent of charge delocalization. This is, in turn, determined by the magnitude of the overlap integral between the two rings. If the  $\pi^*$  orbital is approximated as a linear combination of 2p<sub>z</sub> orbitals of the ring atoms and nonlocal overlaps are neglected, the extent of delocalization is determined by the extent of 2p<sub>z</sub> overlap between the C atoms at the inter-ring C-C bond.<sup>25</sup> For hydrogen-like 2p<sub>z</sub> orbitals,<sup>25a</sup> the overlap integral is given by eq 3.

(24) (a) Wishart, J. F.; Bino, A.; Taube, H. *Inorg. Chem.* **1986**, *25*, 3318. (b) Cotton, F. A.; Wilkinson, G. *Advanced Inorganic Chemistry*; John Wiley & Sons: New York, 1980.

$$\langle 2p_z | 2p_z' \rangle = K^2(2a/Z - L)[\exp(-ZL/2a)] \cos \theta \quad (3)$$

In eq 3,  $K$  is a constant,  $Z$  is the effective nuclear charge, which is constant for a given orbital,  $a$  is the Bohr radius,  $L$  is the distance between the two nuclei, and  $\theta$  is the dihedral angle, the angle displacement between their  $z$  axes. The  $\cos \theta$  term is the origin of the dihedral angle dependence of  $\pi$  electronic coupling. When the two rings are coplanar,  $\theta = 0^\circ$ ,  $\cos \theta = 1$ , and the overlap is maximized. When  $\theta = 47^\circ$ , the magnitude of the overlap integral falls by 32%. When the rings are perpendicular,  $\cos \theta = 0$ , and there is no  $\pi$  electronic delocalization.<sup>25</sup>

In the cation  $[(bpy)Re(CO)_3(MQ^+)]^{2+}$ , the dihedral angle is  $47^\circ$ . It is difficult to assess the effect of crystal packing, but the structure of the crystal near the  $MQ^+$  ligand is relatively open and there is no obvious interaction that would dictate the relative orientations of the two rings. As discussed below, spectral data suggest that the dihedral angle may be, at least, approximately maintained in solution. The maintenance of the dihedral angle at  $47^\circ$  suggests that its magnitude represents a compromise between steric repulsion and electronic delocalization independent of medium.

The effect of electronic coupling appears in the short C-C inter-ring bond length of 1.51 Å. That distance is only slightly longer than the 1.49 Å inter-ring C-C bond in a 4,4'-bpy-bridged Cu(II) dimer where the ligand adopts the planar conformation.<sup>11b</sup> A contributing factor to the inter-ring interaction may come from the  $d\pi-\pi^*(MQ^+)$  back-bonding interaction. Back-bonding leads to partial electronic donation into the  $\pi^*$  system of the  $MQ^+$  ligand. This enhances the contribution of the planar quinoid-like resonance structure involving both rings.<sup>14,15,26</sup> The lowest unoccupied  $\pi^*$  orbital in 4,4'-bpy is strongly bonding at the inter-ring C-C bond.<sup>7,14,15</sup>

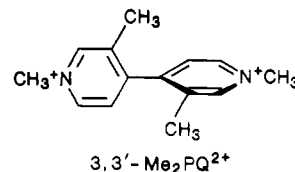
The quinoid structure has been observed by resonance Raman for  $PQ^{+}$ ,<sup>11</sup> 4,4'-bpy<sup>-</sup>,<sup>12</sup> or the biphenyl radical anion<sup>8</sup> where the  $\pi^*$  orbital is fully occupied by one electron. Resonance Raman experiments have also shown that the inter-ring C-C bond has some double-bond character in the MLCT excited state of  $[(NH_3)_5Ru^{II}(4,4'-bpy)]^{2+}$ .<sup>26</sup> Arguments of this kind based on the variation on the extent of charge transfer have been used by several authors to explain the variation in inter-ring C-C bond distances in donor-acceptor salts between  $PQ^{2+}$  and electron-transfer donors in crystals.<sup>13</sup>

**UV-Visible and Electrochemical Properties in Solution. Complexes of Os(II).** In the spectrum of  $[(bpy)_2Os(CO)(4,4'-bpy)]^{2+}$  in Figure 2, the bands that appear at  $\sim 355$  and 412 nm arise from  $d\pi \rightarrow \pi^*(4,4'-bpy)$  and  $d\pi \rightarrow \pi^*(bpy)$  transitions, respectively.<sup>26,27</sup> In  $[(bpy)_2Os(CO)(MQ^+)]^{3+}$  or  $[(bpy)_2Os(CO)(4,4'-bpyH^+)]^{3+}$ , a single broad band appears at  $\lambda_{max} \sim 400$  nm. It includes contributions from overlapping  $d\pi \rightarrow \pi^*(bpy)$  and  $d\pi \rightarrow \pi^*(MQ^+)$  or  $d\pi \rightarrow \pi^*(4,4'-bpyH^+)$  transitions at 420 and  $\sim 390$  nm, respectively.

Protonation or methylation lowers the energy of the  $\pi^*$  orbitals of 4,4'-bpy. MLCT transitions shift to lower energy and ligand-based reductions are shifted to more positive potentials. For  $[(bpy)_2Os(CO)(MQ^+)]^{3+}$  in acetonitrile,  $\mu = 0.1$  M, the first  $MQ^+$ -based reduction occurs at  $-0.67$  V vs SSCE (Table V) compared to the 4,4'-bpy based reduction at  $-1.58$  V in  $[(bpy)_2Os(CO)(4,4'-bpy)]^{2+}$ . By comparison, the reduction potentials for the  $MQ^{+/0}$  and  $PQ^{2+/+}$  couples are  $-0.96$  and  $-0.46$  V under the same conditions.<sup>28</sup> The potential for the  $MQ^{+/0}$  couple in the Os(II) complex is intermediate between the other two. This suggests that although Os(II) binding to the lone pair of the  $MQ^+$  ligand may decrease the energy of  $\pi^*(MQ^+)$ , as does the methylation, the effect is partially counterbalanced by  $d\pi-$

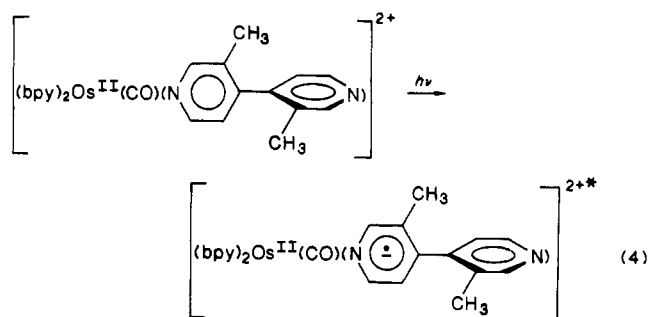
$\pi^*(MQ^+)$  mixing.  $d\pi-\pi^*(MQ^+)$  mixing has the effect of increasing the energy of  $\pi^*(MQ^+)$ .

The importance of electronic coupling between the pyridyl rings also appears in the electrochemical data in Table V. The potential for the first reduction of  $MQ^+$  is 250 mV lower than the potential for the reduction of  $N$ -methylpyridinium ion. It is 320 mV lower for the first reduction of  $PQ^{2+}$  compared to 3,3'-Me<sub>2</sub>PQ<sup>2+</sup> where coplanarity is blocked by the methyl groups in the 3,3'-positions.



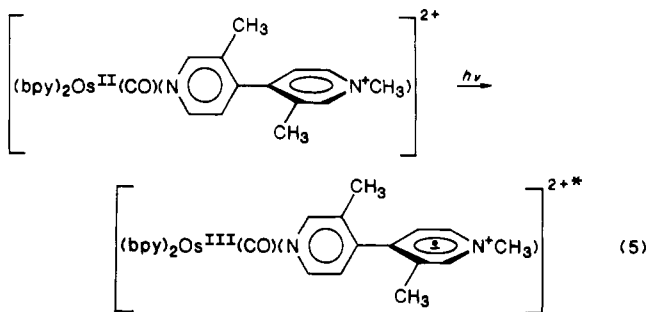
It is 360 mV lower for the pyridinium-based reduction in  $[(bpy)_2Os(CO)(MQ^+)]^{3+}$  compared to  $[(bpy)_2Os(CO)(3,3'-Me_2MQ^+)]^{3+}$ . In all three cases, the greater ease of reduction must reflect, at least in part, the effect of delocalization onto the second ring.

As in the 4,4'-bpy analogue, in  $[(bpy)_2Os(CO)(3,3'-Me_2-4,4'-bpy)]^{2+}$  two MLCT transitions appear,  $d\pi \rightarrow \pi^*(bpy)$  at 416 nm and  $d\pi \rightarrow \pi^*(3,3'-Me_2-4,4'-bpy)$  at  $\sim 335$  nm. The  $d\pi \rightarrow \pi^*(bpy)$  transition occurs at the same energy as in the 4,4'-bpy complex, but the  $d\pi \rightarrow \pi^*(3,3'-Me_2-4,4'-bpy)$  transition is higher in energy by  $\sim 1700$  cm<sup>-1</sup>. It is at higher energy because charge transfer is constrained to occur to the adjacent pyridyl ring. The dependence of MLCT energies on dihedral angle is reminiscent of the spectral shifts observed for the  $\pi \rightarrow \pi^*$  transitions in bridged dicationary salts of 2,2'-bipyridine.<sup>10c,29,30</sup>



The shift to 350 nm in  $[(bpy)_2Os(CO)(3,3'-Me_2MQ^+)]^{3+}$  must be a substituent effect which is transmitted largely through the  $\sigma$ -bonding system of the ligand.<sup>7a</sup>

A charge-transfer transition to the remote pyridinium ring through the adjacent ring as a "bridging ligand" should also exist.



The remote pyridinium site in  $[(bpy)_2Os(CO)(3,3'-Me_2MQ^+)]^{3+}$  is a better oxidant ( $-1.04$  V vs SSCE in CH<sub>3</sub>CN) than is 3,3'-Me<sub>2</sub>-4,4'-bpy in its complex ( $E_{1/2} < -1.9$  V). We have not observed this band. It is expected to be weak because of weak electronic coupling between the rings<sup>31,32</sup> and is probably masked

(25) (a) Levine, I. R. *Quantum Chemistry*; Allen and Bacon, Inc., Boston, MA, 1983. (b) Parr, R. G.; Crawford, B. L. Jr. *J. Chem. Phys.* **1948**, *16*, 526. (c) Dewar, M. J. S. *J. Am. Chem. Soc.* **1952**, *74*, 3345.  
 (26) Caswell, D. S.; Spiro, T. G. *Inorg. Chem.* **1987**, *26*, 18.  
 (27) (a) Schanze, K. S.; Neyhart, G. A.; Meyer, T. J. *J. Phys. Chem.* **1986**, *90*, 2182. (b) Schanze, K. S.; Meyer, T. J. *Inorg. Chem.* **1985**, *24*, 2121.  
 (28) Osa, T.; Kuwana, T. *J. Electroanal. Chem. Interfacial Electrochem.* **1969**, *22*, 389.

(29) (a) Campa, C.; Camps, J.; Font, J.; de March, P. *J. Org. Chem.* **1987**, *52*, 521. (b) Krumholtz, J. *Am. Chem. Soc.* **1951**, *73*, 3487.  
 (30) Amouyal, E.; Zidler, B.; Keller, P.; Moradpour, A. *Chem. Phys. Lett.* **1980**, *74*, 314.  
 (31) (a) Creutz, C. *Prog. Inorg. Chem.* **1983**, *30*, 1. (b) Richardson, D. E.; Taube, H. *J. Am. Chem. Soc.* **1983**, *105*, 40.

by the intense  $d\pi \rightarrow \pi^*(bpy)$  MLCT bands.

**Re(I).** Although the  $\pi \rightarrow \pi^*(bpy)$ ,  $d\pi \rightarrow \pi^*(MQ^+)$ , and  $d\pi \rightarrow \pi^*(bpy)$  bands are badly overlapped for the Re(I) complexes, the difference spectra in Figures 4 and 6 provide clear evidence for the appearance of distinct  $d\pi \rightarrow \pi^*(4,4'-bpy)$  and  $d\pi \rightarrow \pi^*(MQ^+)$  transitions. Giordano and Wrighton found the shift in MLCT  $\lambda_{max}$  in  $(4,4'-bpy)_2Re(CO)_3Cl$  ( $\lambda_{max} = 315$  nm) and  $[(4,4'-bpyH^+)_2Re(CO)_3Cl]^{2+}$  ( $\lambda_{max} = 340$  nm) to be  $2300$   $cm^{-1}$ .<sup>23b</sup> In  $[(MQ^+)_2Re(CO)_3Cl]^{2+}$ , the  $d\pi \rightarrow \pi^*(MQ^+)$  MLCT transition occurs at 355 nm. The shift in energy between the  $d\pi \rightarrow \pi^*(MQ^+)$  and  $d\pi \rightarrow \pi^*(4,4'-bpy)$  transitions is  $\sim 2900$   $cm^{-1}$  in acetonitrile. The  $d\pi \rightarrow \pi^*(3,3'-Me_2,4,4'-bpyH^+)$  transition appears at considerably higher energy than the  $d\pi \rightarrow \pi^*(MQ^+)$  transition, in Figure 4.

**Ru(II).** In the series of complexes  $[(NH_3)_5Ru^{II}(L)]^{2+}$  the shift in  $d\pi \rightarrow \pi^*(L)$  transition energies between L = pyridine or 4-methylpyridine ( $\lambda_{max} = 407$  nm,  $\epsilon \sim 8000$   $M^{-1} cm^{-1}$ ) and L = 4,4'-bpy ( $\lambda_{max} = 478$  nm,  $\epsilon = 12600$   $M^{-1} cm^{-1}$ ) is  $\Delta\bar{\nu} = 3600$   $cm^{-1}$ .<sup>17,26,33-35</sup> Protonation or methylation of the free N atom in 4,4'-bpy causes a further shift to  $\lambda_{max} = 563$  ( $\epsilon = 13800$   $M^{-1} cm^{-1}$ ) and 584 nm ( $\epsilon = 16100$   $M^{-1} cm^{-1}$ ), respectively. A contribution to the decrease in energy in the series L = py > 4,4'-bpy > MQ<sup>+</sup> exists from the increasing extent of electronic delocalization between the rings in the excited state.

The enhanced molar extinction coefficients and associated oscillator strengths are also due to electronic delocalization. The oscillator strength,  $f$ , is related to the transition dipole,  $\bar{\mu}$ , and the transition energy,  $\bar{\nu}$  (in  $cm^{-1}$ ), by eq 6.<sup>36</sup> It is related to the molar

$$f = 1.085 \times 10^{11} \bar{\nu} |\bar{\mu}|^2 \quad (6)$$

absorptivity,  $\epsilon$ , by eq 7. For a Gaussian-shaped absorption band,

$$f = 4.332 \times 10^{-9} \int \epsilon(\bar{\nu}) d\bar{\nu} \quad (7)$$

the oscillator strength is given by eq 8, where  $\epsilon_{max}$  is the molar

$$f = 4.61 \times 10^{-9} \epsilon_{max} \bar{\nu}_{1/2} \quad (8)$$

absorptivity at the band maximum, and  $\bar{\nu}_{1/2}$  is the bandwidth at  $\epsilon = 1/2 \epsilon_{max}$ . It follows from eq 6-8 that the square of the transition dipole is given by eq 9.

$$|\bar{\mu}|^2 = 4.25 \times 10^{-20} (\epsilon_{max} \bar{\nu}_{1/2}) / \bar{\nu} \quad (9)$$

For the  $d\pi \rightarrow \pi^*$  transitions of interest here, the transition dipole moment,  $\bar{\mu}_{CT}$ , is given by eq 10, where  $\Psi_{d\pi}$  is the wave

$$\bar{\mu}_{CT} = \langle \Psi_{\pi^*} | e\bar{r} | \Psi_{d\pi} \rangle \quad (10)$$

function for the metal-based  $d\pi$  electron-donor orbital,  $\Psi_{\pi^*}$  is the wave function for the ligand-based acceptor orbital, and  $e\bar{r}$  is the transition dipole moment operator.<sup>36</sup>

From perturbation theory, the ground- and excited-state wave functions can be written to first order as linear combinations of the "pure"  $d\pi$  and  $\pi^*$  orbitals.<sup>25,31,36</sup>

$$\Psi_{d\pi} = d\pi + \alpha \pi^* \quad (11)$$

$$\Psi_{\pi^*} = \pi^* - \alpha d\pi \quad (12)$$

$$\alpha = \langle \pi^* | \hat{H}' | d\pi \rangle / (E_{d\pi} - E_{\pi^*}) \quad (13)$$

In eq 11-13,  $\alpha$  is the mixing coefficient,  $\hat{H}'$  is the operator that mixes  $d\pi$  and  $\pi^*$ , and  $E_{d\pi}$  and  $E_{\pi^*}$  are the energies of the un-

perturbed  $d\pi$  and  $\pi^*$  orbitals. For relatively weak  $\pi$ -back-bonding interactions,  $\alpha$  is small and the normalization factor is  $\sim 1$ .

Substituting eq 11-13 into eq 10 gives

$$\bar{\mu}_{CT} = \alpha e [\langle \pi^* | \bar{r} | \pi^* \rangle - \langle d\pi | \bar{r} | d\pi \rangle] + e [\langle \pi^* | \bar{r} | d\pi \rangle - \alpha^2 \langle d\pi | \bar{r} | \pi^* \rangle] \quad (14)$$

For the relatively strong MLCT transitions of interest here, the last two terms are negligible compared to the first two terms. This gives eq 15, where  $\langle d\pi | \bar{r} | d\pi \rangle$  and  $\langle \pi^* | \bar{r} | \pi^* \rangle$  are the radial ex-

$$\bar{\mu}_{CT} = \alpha e [\langle \pi^* | \bar{r} | \pi^* \rangle - \langle d\pi | \bar{r} | d\pi \rangle] = \alpha e \bar{R} \quad (15)$$

pectation values for the excited electron in the unperturbed  $d\pi$  and  $\pi^*$  orbitals and  $\bar{R}$  is the transition dipole length.

When written as a linear combination of the 2p orbitals of the N and C atoms of the ring, the  $\pi^*$  acceptor orbital is given by eq 16.<sup>31b</sup> The coefficients  $a$  are the appropriate weighting factors

$$\pi^* = a_N 2p_N + a_{C,1} 2p_{C,1} + a_{C,2} 2p_{C,2} + \dots \quad (16)$$

for the 2p orbitals of the N atom bound to the metal and various carbon atoms in the ring.  $2p_N$ ,  $2p_{C,1}$ ,  $2p_{C,2}$ , etc. are the corresponding wave functions. Since the C atoms in the ring are remote from the metal, their overlaps with  $d\pi$  are negligible.<sup>31b</sup> This leads to the expression for  $\alpha$  and  $\bar{\mu}_{CT}$  in eq 17 and 18.

$$\alpha = a_N \langle 2p_N | \hat{H}' | d\pi \rangle / (E_{d\pi} - E_{\pi^*}) = a_N \beta / \Delta E \quad (17)$$

$$\bar{\mu}_{CT} = \sqrt{2} e a_N \beta \bar{R} / \Delta E \quad (18)$$

In comparing the MLCT transitions for py vs 4,4'-bpy as the acceptor ligand, the resonance integral,  $\beta$ , should be nearly the same and  $\Delta E \sim \bar{\nu}$  if the extent of mixing between  $d\pi$  and  $\pi^*$  is small. Assuming constant bandwidths, it follows from eq 9 and 18 that the ratio of transition dipole lengths is given by eq 19.

$$\frac{|\bar{R}_{bpy}|}{|\bar{R}_{py}|} = \left( \frac{\bar{\nu}_{bpy} \epsilon_{max,bpy}}{\bar{\nu}_{py} \epsilon_{max,py}} \right)^{1/2} \frac{a_{N,py}}{a_{N,bpy}} \quad (19)$$

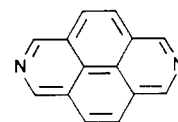
Substituting the measured molar extinction coefficients and absorption band energies into eq 19 gives eq 20.<sup>33</sup> From the results

$$|\bar{R}_{bpy}| / |\bar{R}_{py}| = 1.08 (a_{N,py} / a_{N,bpy}) \quad (20)$$

of molecular orbital calculations on the two ligands based on the CNDO method,<sup>33c</sup>  $a_{N,py} = 0.59$  and  $a_{N,bpy} = 0.40$ , which gives  $|\bar{R}_{bpy}| / |\bar{R}_{py}| \sim 1.7$ . On the basis of this calculation, the dipole length for L = 4,4'-bpy is greater by a factor of 1.7, which is also consistent with a  $\pi^*$ -acceptor orbital that extends onto the remote pyridyl ring of 4,4'-bpy.

For the MLCT transition in  $[(NH_3)_5Ru^{II}(4,4'-bpyH^+)]^{3+}$  compared to its unprotonated analogue, there is a red shift of  $\sim 3200$   $cm^{-1}$  but only a slight enhancement in band intensity from 12600 to 13800  $M^{-1} cm^{-1}$ . The electrostatic effect of methylation or protonation lowers the energy of the  $\pi^*$ -acceptor orbital and leads to further electronic delocalization onto the remote pyridinium ring. These changes appear as decreased values of  $\Delta E$  and  $a_N$  in eq 18 and 19. The decreases in the two compensate, leaving the band intensity nearly constant. For  $[(NH_3)_5Ru^{II}(3,3'-Me_2-4,4'-bpyH^+)]^{3+}$  the high-energy (450 nm) and lowered intensity ( $\epsilon = 5000$   $M^{-1} cm^{-1}$ ) for the  $d\pi \rightarrow \pi^*$  transition are consistent with a transition that is localized to the adjacent ring.

Our conclusions concerning electronic delocalization are consistent with a number of earlier observations.<sup>31,32</sup> For the mixed-valence complexes  $[(NH_3)_5Ru^{III}(L)Ru^{II}(NH_3)_5]^{5+}$ , the intervalence (IT) transition for L = 4,4'-bpy is nearly equal in intensity to that for L = 2,7-diazapyrene. However, it is far more



2,7-diazapyrene

intense than the IT band for L = 3,3'-Me<sub>2</sub>-4,4'-bpy.<sup>31</sup> In

- (32) Fischer, H.; Tom, G. M.; Taube, H. *J. Am. Chem. Soc.* **1976**, *98*, 5512.  
 (33) (a) Ford, P. C.; Rudd, De F. P.; Gaunder, R.; Taube, H. *J. Am. Chem. Soc.* **1968**, *90*, 1187. (b) Chassignan, D. A.; Hintze, R. E.; Stuemmer, D. H.; Petersen, J. D.; McDonald, D. P.; Ford, P. C. *J. Am. Chem. Soc.* **1972**, *94*, 6665. (c) Lavalley, D. K.; Fleischer, E. B. *J. Am. Chem. Soc.* **1972**, *94*, 2583, 2599. (d) Curtis, J.; Sullivan, B. P.; Meyer, T. *J. Inorg. Chem.* **1983**, *22*, 224. (e) Sutton, J. E.; Taube, H.; *Inorg. Chem.* **1981**, *20*, 3125.  
 (34) Atalla, M. L.; Lawrance, G. L.; Summers, L. A. *Transition Met. Chem. (Weinheim, Ger.)* **1985**, *10*, 354.  
 (35) Winkler, J. R.; Netzel, T. L.; Creutz, C.; Sutin, N. *J. Am. Chem. Soc.* **1987**, *109*, 2381.  
 (36) (a) Ballhausen, C. J. *Molecular Electronic Structures of Transition Metal Complexes*, McGraw-Hill, Inc.: London, 1979. (b) Mulliken, R. S.; Person, W. B. *Molecular Complexes*; John Wiley & Sons, Inc.: New York, 1969. (c) Mulliken, R. S. *J. Am. Chem. Soc.* **1952**, *74*, 811. (d) Day, P.; Sanders, N. *J. Chem. Soc. A* **1967**, 1536.



$[(\text{NH}_3)_5\text{Ru}^{\text{II}}(\text{L})^{2+}]$  the shifts in ligand-localized  $\pi-\pi^*$  and MLCT band energies upon protonation are of the same magnitude for  $\text{L} = 4,4'$ -bpy or pyrazine. This suggests that a nearly planar conformation for protonated  $4,4'$ -bpy exists in the ground state of  $[(\text{NH}_3)_5\text{Ru}^{\text{II}}(4,4'\text{-bpyH}^+)]^{3+}$ .<sup>33c</sup> Picosecond transient absorption techniques have been used to establish the charge-transfer character of the lowest-lying excited state in  $[(\text{NH}_3)_5\text{Ru}^{\text{II}}(4,4'\text{-bpy})]^{2+}$ . The appearance of transient absorbance maxima at 360 and 580 nm is consistent with the excited electron being delocalized over both of the pyridyl rings in the thermally equilibrated excited state.<sup>33b,35</sup>

**Effects of Rigid Media.** The temperature dependence of the absorption spectra of  $[(\text{bpy})_2\text{Os}(\text{CO})(\text{MQ}^+)]^{3+}$ ,  $[(\text{MQ}^+)_2\text{Re}(\text{CO})_3\text{Cl}]^{2+}$ , and  $[(\text{bpy})\text{Re}(\text{CO})_3(\text{MQ}^+)]^{2+}$  in 4:1 (v/v) EtOH/MeOH are shown in Figures 3 and 5. The decreases in bandwidth with temperature occur as the average energy of the surrounding librational modes decreases.<sup>36a,37</sup> Part of the increase in intensity is due to the contraction of the solution, which can be up to  $\sim 30\%$  between room temperature and 77 K.<sup>37</sup>

The MLCT transition energy for  $[(\text{MQ}^+)_2\text{Re}(\text{CO})_3\text{Cl}]^{2+}$  is only slightly temperature dependent. The absorption energy in EtOH/MeOH is nearly the same in fluid solution and in the glass at 100 K. From the difference spectra for  $[(\text{bpy})\text{Re}(\text{CO})_3(\text{MQ}^+)](\text{PF}_6)_2$  and  $[(\text{bpy})\text{Re}(\text{CO})_3(4\text{-Etpy})](\text{PF}_6)$  in KBr pellets, in the glass and in solution, the  $d\pi \rightarrow \pi^*(\text{MQ}^+)$  transition occurs at nearly the same energy,  $\sim 340$  nm, in all three media. The near constancy of the  $d\pi \rightarrow \pi^*(\text{MQ}^+)$  transition energies in the three different media suggests that the extent of electronic delocalization between the rings is relatively unaffected by the medium. By inference, the dihedral angle between the rings may close to  $47^\circ$  in all three media for  $[(\text{bpy})\text{Re}(\text{CO})_3(\text{MQ}^+)]^{2+}$ .

**Excited-State Energetics.** In the complex  $[(\text{bpy})\text{Re}(\text{CO})_3(\text{MQ}^+)]^{2+}$ , the  $\text{MQ}^+$  ligand is a better electron acceptor than bpy by  $\sim 0.44$  V based on the electrochemical results in Table V. As expected from these results, emission from the *thermally equilibrated*  $d\pi-\pi^*(\text{MQ}^+)$  excited state in  $[(\text{bpy})\text{Re}(\text{CO})_3(\text{MQ}^+)]^{2+}$  occurs at lower energy than emission from the  $d\pi-\pi^*(\text{bpy})$ -based excited state of  $[(\text{bpy})\text{Re}(\text{CO})_3(4\text{-Etpy})]^+$  by  $3400\text{ cm}^{-1}$  (0.42 eV).<sup>2</sup>

In both the electrochemical and emission experiments, an electron has been added to the  $\text{MQ}^+$  ligand and the two pyridyl rings are coplanar,  $\theta \sim 0^\circ$ . Application of the Franck-Condon principle shows that the situation is different for light absorption. The time scale for electronic excitation by light absorption is shorter than the time scale for intramolecular structural changes such as rotation around the dihedral angle. Direct  $d\pi \rightarrow \pi^*(\text{MQ}^+)$  excitation in  $[(\text{bpy})\text{Re}(\text{CO})_3(\text{MQ}^+)]^{2+}$  gives the excited state in the  $\theta = 47^\circ$  configuration of the ground state rather than the  $\theta = 0^\circ$  configuration of the equilibrated excited state. This increases the energy of the  $d\pi \rightarrow \pi^*(\text{MQ}^+)$  transition. This effect is sufficiently large that with  $\theta$  frozen at  $\sim 47^\circ$  the ordering of the transition energies is inverted with the  $d\pi \rightarrow \pi^*(\text{bpy})$  transition lying lower than the  $d\pi \rightarrow \pi^*(\text{MQ}^+)$  transition by  $1200\text{ cm}^{-1}$  (0.15 eV). The energy of the  $d\pi \rightarrow \pi^*(\text{MQ}^+)$  state is highly dependent upon the dihedral angle.

Emission energies,  $E_{\text{em}}$ , for  $d\pi \rightarrow \pi^*(\text{bpy})$  emission in  $[(\text{bpy})\text{Re}(\text{CO})_3(4\text{-Etpy})]^+$  or  $d\pi \rightarrow \pi^*(\text{MQ}^+)$  emission in  $[(\text{bpy})\text{Re}(\text{CO})_3(\text{MQ}^+)]^{2+}$  are given by eq 21 in the classical limit.<sup>38</sup>

$$E_{\text{em}} = \Delta G_{\text{ES}} - \lambda_0 - \lambda_1 = \Delta G_{\text{ES}} - \lambda \quad (21)$$

In eq 21,  $\Delta G_{\text{ES}}$  is the free energy of the *equilibrated* excited state above the ground state.  $\lambda_0$  and  $\lambda_1$  are the solvent and intramolecular reorganizational energies. Equation 21 assumes that the frequencies of the vibrational and librational modes that respond to the change in electronic configuration between states remain constant. The difference in energy between the  $d\pi \rightarrow \pi^*(\text{bpy})$  and  $d\pi \rightarrow \pi^*(\text{MQ}^+)$  emitters is given by eq 22. Similarly, the

$$\Delta E_{\text{em}} = E_{\text{em,bpy}} - E_{\text{em,MQ}^+} = (\Delta G_{\text{ES,bpy}} - \Delta G_{\text{ES,MQ}^+}) - (\lambda_{\text{bpy}} - \lambda_{\text{MQ}^+}) = \Delta(\Delta G_{\text{ES}}) - \Delta\lambda \quad (22)$$

energy of  $d\pi \rightarrow \pi^*(\text{bpy})$  absorption is given by eq 23, the  $d\pi \rightarrow \pi^*(\text{MQ}^+)$  absorption by eq 24, and the difference between them by eq 25.  $E(\theta)$  is the increase in energy associated with increasing

$$E_{\text{abs,bpy}} = \Delta G_{\text{ES,bpy}} + \lambda_{0,\text{bpy}} + \lambda_{1,\text{bpy}} = \Delta G_{\text{ES,bpy}} + \lambda_{\text{bpy}} \quad (23)$$

$$E_{\text{abs,MQ}^+} = \Delta G_{\text{ES,MQ}^+} + \lambda_{0,\text{MQ}^+} + \lambda_{1,\text{MQ}^+} + E(\theta) = \Delta G_{\text{ES,MQ}^+} + \lambda_{\text{MQ}^+} + E(\theta) \quad (24)$$

$$\Delta E_{\text{abs}} = E_{\text{abs,bpy}} - E_{\text{abs,MQ}^+} = \Delta(\Delta G_{\text{ES}}) - E(\theta) + \Delta\lambda \quad (25)$$

the dihedral angle from  $\theta = 0^\circ$ . It includes a contribution from the loss of electronic delocalization between the rings and, if there is a change in the electron transfer distance with  $\theta$ , a contribution from the change in  $\lambda_0$ . It follows from the difference between  $\Delta E_{\text{em}}$  and  $\Delta E_{\text{abs}}$  that

$$E(47^\circ) = \Delta E_{\text{em}} - \Delta E_{\text{abs}} + 2\Delta\lambda = 0.57\text{ eV} + 2\Delta\lambda \quad (26)$$

The solvent reorganizational energies are dependent upon the extent of electronic radial redistribution in the transition. Because of the greater charge-transfer distance for the  $d\pi \rightarrow \pi^*(\text{MQ}^+)$  transition,  $\lambda_{0,\text{MQ}^+} > \lambda_{0,\text{bpy}}$ ,  $\Delta\lambda_0$  is negative and,  $E(47^\circ) \leq 0.57$  eV. The same analysis applied to  $[(\text{bpy})_2\text{Os}(\text{CO})(\text{MQ}^+)]^{3+}$  gives the excess energy in the "twisted"  $d\pi \rightarrow \pi^*(\text{MQ}^+)$  transition to be  $\leq 0.65$  eV.

**Intramolecular Quenching and Related Processes.** The results described here were obtained in an attempt to understand why intramolecular  $\pi^*(\text{bpy}) \rightarrow \pi^*(\text{MQ}^+)$  electron transfer in  $[(\text{bpy})\text{Re}(\text{CO})_3(\text{MQ}^+)]^{2+}$  and  $[(\text{bpy})_2\text{Os}(\text{CO})(\text{MQ}^+)]^{3+}$  is inhibited in a frozen solution or glass. There are two nearly classical motions that respond to the difference in electronic configuration between the states  $[(\text{bpy}^-)\text{Re}^{\text{II}}(\text{CO})_3(\text{MQ}^+)]^{2+}$  and  $[(\text{bpy})\text{Re}^{\text{II}}(\text{CO})_3(\text{MQ}^+)]^{2+}$ . One is solvent dipole reorientation. The other is rotation about the dihedral angle from  $\theta = 47^\circ$  to  $\theta = 0^\circ$ . It seems doubtful that rotation plays an important dynamic role in the intramolecular electron transfer in reaction 2 in fluid solution. Measurements on related organic systems suggest that the time scales for such motions in fluid solution are exceedingly short ( $< 30$  ps).<sup>39</sup> Although the mode could be inhibited in the glass, it appears not to be in the complex  $[(4,4'\text{-}(\text{NH}_2)_2\text{bpy})\text{Re}(\text{CO})_3(\text{MQ}^+)]^{2+}$ . In this complex emission from the equilibrated  $d\pi \rightarrow \pi^*(\text{MQ}^+)$  state is observed in the glassy stage at low temperature.<sup>2a</sup>

The requirement for solvent dipole reorientation does inhibit electron transfer in the glass.<sup>2a,40</sup> The role of the solvent dipole reorientation is illustrated in the energy coordinate diagram in Figure 7. The coordinate shown in the diagram is that for an averaged librational mode, which is assumed to be a harmonic oscillator.<sup>41</sup>

Before optical excitation, the solvent dipoles surrounding the complex have average orientations appropriate to the electronic configurations of the ground state. Application of the Franck-Condon principle shows that light absorption is a vertical transition with the solvent dipoles remaining in the average orientations of the ground state. In fluid solution,  $d\pi \rightarrow \pi^*(\text{bpy})$  excitation is followed by rapid reorientation of the solvent dipoles to orientations that, on the average, are appropriate to the  $(d\pi)^5(\pi^*)^1$  electronic configuration of the excited state. The change in equilibrium displacement for the librational mode between the ground and

(37) (a) Meyer, B. *Low Temperature Spectroscopy*; Elsevier: New York, 1971. (b) Willard, J. E. *J. Phys. Chem.* **1975**, *79*, 2966.

(38) (a) Hush, N. *Prog. Inorg. Chem.* **1967**, *8*, 391. (b) Bunschwig, B. S.; Ehrenson, S.; Sutin, N. *J. Phys. Chem.* **1987**, *91*, 4714.

(39) (a) Maroncelli, M.; Castner, E. W.; Webb, S. P.; Fleming, G. R. In *Ultrafast Phenomena*; Fleming, G. R., Seigman, A., Eds.; Springer: Berlin, 1986; Vol. 5, p 293. (b) Koll, A.; Kolodziej, H. A.; Sorriso, S. *Z. Phys. Chem.* **1983**, *134*, 163. (c) Freundlich, P.; Jakusek, E.; Kolodziej, H. A.; Pajdowska, M.; Sorriso, S. *J. Phys. Chem.* **1983**, *87*, 1034. (d) Ribeiro-Claro, P. J. A.; Amorin da Costa, A. M.; Teixeira-Dias, J. J. C. *J. Raman Spectrosc.* **1987**, *18*, 497.

(40) (a) Lumpkin, R. S.; Meyer, T. J. *J. Phys. Chem.* **1986**, *90*, 5307. (b) Danielson, E.; Lumpkin, R. S.; Meyer, T. J. *J. Phys. Chem.* **1987**, *91*, 1305. (c) Kitamura, N.; Kim, H. B.; Kawanishi, Y.; Obata, Y.; Tazuke, S. *J. Phys. Chem.* **1986**, *90*, 1488.

(41) (a) Levich, V. G. *Adv. Electrochem. Electrochem. Eng.* **1966**, *4*, 249. (b) Kestner, N. R.; Logan, J.; Jortner, J. *J. Phys. Chem.* **1974**, *78*, 2148.

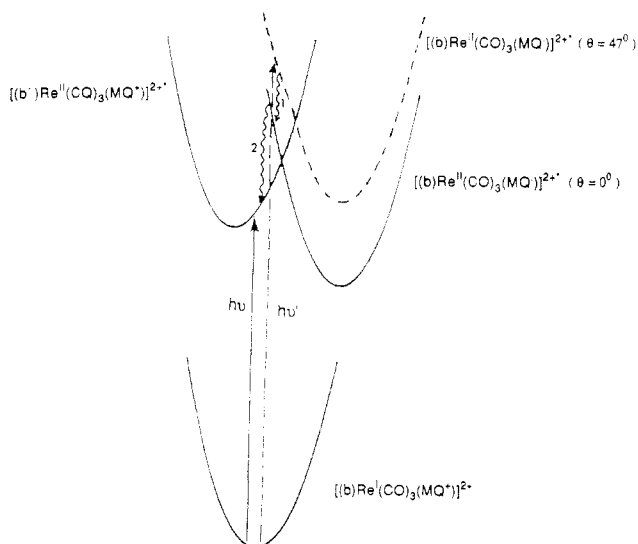
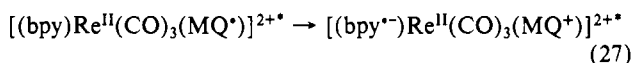


**Figure 7.** Energy-coordinate diagram for an averaged solvent librational mode, approximated as a harmonic oscillator, for the excited and ground states of  $[(bpy)Re(CO)_3(MQ^+)]^{2+}$  ( $b = bpy$ ). The dashed line,  $h\nu'$ , illustrates the vertical  $d\pi \rightarrow \pi^*(MQ^+)$  transition with the dihedral angle between the rings at the ground-state value of  $47^\circ$ .

$d\pi \rightarrow \pi^*$  excited states is a consequence of the change in radial electronic distribution between states. The change in displacement is shown as being greater for the  $d\pi \rightarrow \pi^*(MQ^+)$  state than for the  $d\pi \rightarrow \pi^*(bpy)$  state. This is based on the greater transition length for  $d\pi \rightarrow \pi^*(MQ^+)$  state. The magnitude of  $\lambda_0$  and the extent of solvent dipole reorientation will increase with the charge-transfer distance.<sup>3</sup>

High-energy light absorption into the  $d\pi \rightarrow \pi^*(MQ^+)$  transition ( $h\nu'$  in Figure 7) leads to the nonequilibrium  $d\pi \rightarrow \pi^*(MQ^+)$  excited state with  $\theta = 47^\circ$ . In Figure 7, it is assumed that initial excitation is followed by rapid intramolecular vibrational relaxations including the change from  $\theta = 47^\circ$  to  $\theta = 0^\circ$ , process 1 in Figure 7. In fluid solution a further relaxation occurs along the librational coordinate to give the fully equilibrated excited state.

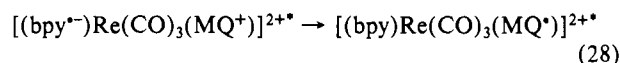
In a glass, the solvent dipoles are frozen and *librational relaxation can not occur on the time scale of the excited state lifetime*. Excited state decay of the nonequilibrated state can occur via radiative or nonradiative channels. As shown as process 2 in Figure 7, it can also undergo nonradiative decay to the  $d\pi \rightarrow \pi^*(bpy)$  state if the  $d\pi \rightarrow \pi^*(bpy)$  state is lower in energy. The existence of this process explains why  $d\pi \rightarrow \pi^*(MQ^+)$  excitation of  $[(bpy)Re(CO)_3(MQ^+)]^{2+}$  leads to  $d\pi \rightarrow \pi^*(bpy)$  emission (reaction 27). The  $d\pi \rightarrow \pi^*(MQ^+) \rightarrow d\pi \rightarrow \pi^*(bpy)$  decay process is the



inverse of the intramolecular  $bpy \rightarrow MQ^+$  electron transfer in reaction 2.

In the glass, the electron-transfer reaction that interconverts the upper and lower MLCT excited states can occur with net energy conservation. There is an energy loss in the librational modes when process 2 occurs. The energy loss appears in the  $Re^{II}(bpy^-)$  MLCT state as excess vibrational energy in the intramolecular modes that respond to the change in electronic configuration between the  $d\pi \rightarrow \pi^*(MQ^+)$  and  $d\pi \rightarrow \pi^*(bpy)$  states.

The intramolecular electron transfer in reaction 28 cannot occur in the glass. The solvent dipoles are orientationally frozen, and



thermally activated crossing of the librational barrier in Figure 7 cannot occur.<sup>2a</sup> The solvent librational modes have small quantum spacings,  $1\text{--}10\text{ cm}^{-1}$ , and are nearly classical in nature. The difference in the equilibrium displacements between the  $d\pi \rightarrow \pi^*(bpy)$  and  $d\pi \rightarrow \pi^*(MQ^+)$  states are large so that the nuclear tunneling probability through the librational barrier is small. In fluid solution, thermally activated classical crossing over the librational barrier can occur because thermal fluctuations lead to the required changes in the solvent dipole orientations.

Following the vertical transitions  $h\nu$  and  $h\nu'$  in Figure 7 and relaxation of the intramolecular modes, the energies of the  $d\pi \rightarrow \pi^*(bpy)$  and  $d\pi \rightarrow \pi^*(MQ^+)$  states are given by  $\Delta G^\circ(bpy) + \lambda_0(bpy)$  and  $\Delta G^\circ(MQ^+) + \lambda_0(MQ^+)$ .  $\Delta G^\circ(bpy)$  and  $\Delta G^\circ(MQ^+)$  are the free energies of the equilibrated excited states above the ground states.  $\lambda_0(bpy)$  and  $\lambda_0(MQ^+)$  are the solvent dipole reorganizational energies between the excited states and the ground state. The quantities  $\Delta G + \lambda_0$  are the energies of the equilibrated excited states in the frozen dipole environment of the glass. The excited states are equilibrated in the intramolecular vibrations but remain surrounded by the solvent dipole orientations of the ground state.

In terms of these energy quantities, intramolecular electron transfer can not occur in the glassy state, if  $\Delta G^\circ(bpy) + \lambda_0(bpy) < \Delta G^\circ(MQ^+) + \lambda_0(MQ^+)$ .<sup>2a</sup> In this case there is necessarily a librational barrier to  $bpy \rightarrow MQ^+$  electron transfer. If  $\Delta G^\circ(bpy) + \lambda_0(bpy) > \Delta G^\circ(MQ^+) + \lambda_0(MQ^+)$ , there is no librational barrier, the energy released in the transition appears in the intramolecular vibrational modes and electron transfer can occur in the glass.

**Acknowledgment** is made to the National Science Foundation for financial support under Grant No. CHE-8503092.

**Registry No.**  $PQ^{2+}$ , 4685-14-7;  $3,3'\text{-Me}_2PQ^{2+}$ , 83133-28-2;  $[(bpy)Re(CO)_3(MQ^+)](PF_6)_2$ , 120521-03-1;  $[(bpy)_2Os(CO)(py)]^{2+}$ , 89689-79-2;  $[(bpy)_2Os(CO)(MQ^+)]^{3+}$ , 120418-56-6;  $[(bpy)_2Os(CO)(3,3'\text{-Me}_2MQ^+)]^{3+}$ , 120418-57-7;  $[(bpy)Re(CO)_3(4\text{-Etpy})]^+$ , 84028-68-2;  $[(MQ^+)_2Re(CO)_3Cl]^{2+}$ , 120418-58-8;  $[(bpy)Re(CO)_3(MQ^+)]^{2+}$ , 86695-84-3;  $[(bpy)_2Os(CO)(4,4'\text{-bpy})]^{2+}$ , 96503-60-5;  $[(bpy)_2Os(CO)(3,3'\text{-Me}_2,4,4'\text{-bpy})]^{2+}$ , 120418-59-9;  $[(bpy)Re(CO)_3(4,4'\text{-bpy})]^+$ , 120418-60-2;  $[(bpy)Re(CO)_3(3,3'\text{-Me}_2,4,4'\text{-bpy})]^+$ , 120418-61-3.

**Supplementary Material Available:** Tables of anisotropic thermal parameters (Table S1) and hydrogen atom positional parameters (Table S2) (4 pages). Ordering information is given on any current masthead page.